




Cite this: *J. Mater. Chem. B*, 2018, 6, 5460

Real-time tracking of the autophagy process in living cells using plasmonically enhanced Raman spectroscopy of fucoidan-coated gold nanoparticles†

Hongje Jang, *^{ab} Kyungtae Kang‡^c and Mostafa A. El-Sayed*^a

To date, a variety of biological assays such as immunostaining, western blotting, enzyme-linked immunosorbent assay (ELISA), and flow cytometry have been used to analyze and trace important biological events and therapies. In addition to these techniques, the application of microscopic analytical techniques such as matrix-assisted laser desorption/ionization-time of flight (MALDI-ToF) mass spectrometry and Raman spectroscopy is increasing, allowing information to be obtained at the molecular level. In this study, we have conducted real-time tracking of autophagy, a cellular process that has recently been attracting significant attention. To achieve this purpose, we performed Raman spectroscopy on human oral squamous carcinoma cells (HSC3) incubated with bioactive molecule-modified plasmonic gold nanoparticles. The bioactive molecule–nanoparticle complexes were synthesized using fucoidan, a biopolymer that induces autophagy. By using this platform, it was possible to trace the entire autophagic process successively from cell introduction to autophagic apoptosis. This fusion of nanocomposites and spectroscopic techniques is expected to enable more complex biological processes to be pursued at the molecular level in the future.

Received 29th May 2018,
Accepted 10th August 2018

DOI: 10.1039/c8tb01402g

rsc.li/materials-b

1 Introduction

Autophagy, also referred to as self-digestion or intracellular recycling, was the mainstay of the 2016 Nobel Prize in Physiology. The term autophagy is derived from Greek meaning ‘self-devouring’. It can be summarized as the process by which damaged cell components or organelles, or components that are no longer needed, are broken down in order to recycle them to maintain the energy balance, particularly in response to critical stresses such as starvation.^{1–6} Since the first report of this process by the Belgian biochemist Christian de Duve, many researchers have spent the last 50+ years unraveling different autophagic mechanisms and their regulation.⁷ Several types of autophagy are now known to exist depending on the mechanism, but commonly autophagy begins with an ‘isolation membrane’ step by which target molecules or organelles are encapsulated by a lipid bilayer derived from the endoplasmic reticulum (ER) or the *trans*-Golgi. As a result of this process, a vesicle called the autophagosome is formed, which surrounds and contains the

cellular material destined for degradation. The autophagosome then fuses with the lysosome, which is responsible for intracellular degradation, resulting in processing of the targeted cellular material into molecules that can be used as energy sources. As a result of the autophagic process, and the resulting decomposition of unnecessary or harmful substances, cells are able to survive. However, excessive autophagy can induce cell apoptosis rather than cell survival. This type of cell death is referred to as autophagic cell death or autophagic apoptosis (type II cell death), and it differs from conventional apoptosis or necrosis (type I cell death).^{8,9} Autophagy is a biological event that has been actively studied since it relates to the enhancement of immunity and the prevention of aging as well as the treatment of various diseases including cancer.^{10–15}

The various biological events that occur during autophagy have been identified and characterized using a range of commonly used analytical techniques including gel electrophoresis, western blotting, and flow cytometry.^{16–20} However, these analytical techniques are not suitable for real-time observation since they are end-point measurements. To overcome the limitation of this type of analysis, single molecule microscopy or time-resolved cellular imaging approaches have recently been developed. However, the development of new analytical techniques is still required for real-time monitoring at the molecular level. To meet this requirement, our group has applied plasmonically enhanced Raman spectroscopy (PERS) to perform real-time monitoring of specific biological events in live cells. PERS is a

^a Laser Dynamics Laboratory, School of Chemistry and Biochemistry, Georgia Institute of Technology, Atlanta, GA30332, USA. E-mail: melsayed@gatech.edu

^b Department of Chemistry, Kwangwoon University, 20 Gwangun-ro, Nowon-gu, Seoul, Republic of Korea. E-mail: hjang@kw.ac.kr

^c Department of Applied Chemistry, Kyung Hee University, Yongin, Gyeonggi 17104, Republic of Korea

† Electronic supplementary information (ESI) available. See DOI: 10.1039/c8tb01402g

‡ These authors contributed equally.

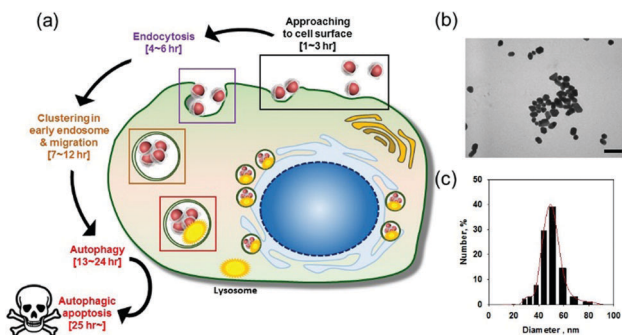


Fig. 1 (a) Schematic illustration of Fu-AuNP mediated real-time autophagy tracking. (b) TEM and (c) DLS characterization of the prepared Fu-AuNPs. The scale bar is 100 nm.

generic term for various plasmon-based Raman signal enhancement techniques, including roughened metal nanostructure surface enhanced Raman spectroscopy (SERS) of adsorbed analytes. This is not limited to the surface or hot spot of a single nanostructure but can be implemented according to an environmentally created geometric position such as intact nanoparticle gaps or holes of clustered nanostructures and has been recently utilized for a biological event at a molecular level.²¹⁻²³ Effective plasmon nanoparticle-based PERS shows high efficacy when the localized surface plasmon resonance (LSPR) and excitation laser wavelength are in a similar range, and nanoparticles of various sizes and morphologies have been developed for this purpose.²⁴ The effectiveness of real-time monitoring using PERS has already been confirmed by successful tracking of cell apoptosis, photo-thermal conversion mediated hyperthermia, and ultraviolet (UV) radiation-induced cell responses. Based on this, we anticipated that the PERS approach could be used for molecular-level tracking of autophagy dynamics.²⁵⁻²⁷

Here, we report the real-time tracking of autophagy dynamics in living cells using PERS combined with fucoidan-coated gold nanoparticles (Fu-AuNPs) (Fig. 1a). Fucoidan, a brown seaweed *mozuku* extract, is a sulfated carbohydrate that has autophagy-triggering, anti-cancer, and anti-bacterial activity and is commonly used as a nutritional supplement as well as being used in research.^{28,29} Because of its ability to induce autophagic apoptosis, fucoidan was chosen as the reducing agent and surface coating biopolymer for the formation of plasmonic Fu-AuNPs to generate a PERS probe. Using the Fu-AuNPs, and with real time Raman measurements taken over 28 h, the entire autophagocytic process, from induction to apoptosis, could be followed at the molecular level in a human squamous carcinoma cell line. The current report is the first describing the real-time observation of autophagy using Raman spectroscopy and has expanded the scope of studies at the molecular level capable of observing biological events in real-time.

2 Experimental

2.1 Materials

Hydrogen tetrachloroaurate(III) hydrate, trisodium citrate dehydrate, sodium chloride, sodium hydroxide, pyridine, formamide, hydrogen chloride, acetic anhydride, Hoechst 33342 and XTT were purchased

from Sigma-Aldrich (Milwaukee, WI, USA). Mozuku fucoidan extract powder was purchased from Okinawa agent (Itoman, Japan). 10× phosphate-buffered saline (PBS), Dulbecco's modified Eagle's medium (DMEM) supplemented with 4.5 g L⁻¹ glucose and sodium pyruvate, fetal bovine serum (FBS) and antimycotic solution were purchased from VWR (Randor, PA, USA). The Promo autophagy sensor LC3B-RFP Bacmam 2.0 was purchased from Life technology (Grand Island, NY, USA). All chemicals were used as received.

2.2 Synthesis of Fu-AuNPs

Fucoidan was dissolved in DI water to prepare a 10 wt% stock solution. The solution was diluted to 1.5 wt% into the DI water with a total volume of 20 mL in a glass vial, then heated up to 80 °C on a heat plate. To the sufficiently heated fucoidan solution, 20 μL of hydrogen tetrachloroaurate(III) hydrate stock solution (0.1 g mL⁻¹) was added and heated for an additional 2 h. During this incubation step, the color of the reaction mixture turned deep red. The manufactured Fu-AuNP solution was then cooled to room temperature, then purified by centrifugation for 20 min at 8000 rpm. The product was rinsed with DI water 4 times to remove the remaining chemicals. Finally, the synthesized Fu-AuNPs were re-dispersed in DI water and characterized by using a UV-Vis spectrophotometer, and then stored at room temperature. The Fu-AuNPs should be consumed within a month to prevent aggregation from colloidal stability decrement.

2.3 Characterization of the synthesized nanoparticles

A JEOL TEM 100CX (JEOL, USA) was used to obtain images of the AuNPs. Fluorescence images of the cells were collected by a Zeiss LSM 700-405 confocal microscope (Carl Zeiss Inc., Oberkochen, Germany). The hydrodynamic radius was characterized by a Zetasizer Nano ZS (Malvern, UK) in a triplicate manner with calculation through the Stokes-Einstein equation. Absorbance measurement during the XTT assay was performed by a SynergyMx (BioTek, UK).

2.4 Surface modification of Fu and Fu-AuNPs

Human oral squamous cell carcinoma (HSC3) cells were cultured in Dulbecco's modified Eagle's medium supplemented with 4.5 g L⁻¹ glucose and sodium pyruvate, 10% v/v fetal bovine serum and 1% antimycotic solution. Cell cultures were maintained at 37 °C in a 5% CO₂ humidified incubator.

2.5 Cell viability assay

HSC3 cells were seeded with a density of 5000 cells per well into a 96-well culture plate with 100 μL of growth medium (about 50% confluency). After the successful cell attachment by 1 day incubation, nanoparticles or drug-nanoparticles were added to conduct the cell viability assignment. The cells were incubated for an additional 24 or 48 h under incubation conditions (37 °C, 5% CO₂ humidity), and the cells were rinsed with 1× PBS. 50 μL of activated XTT solution (XTT solution + activation reagent) was added to each well and the plate was incubated in an incubator for an additional 4 h. The plate was shaken gently to

evenly distribute the dye in the wells, then the absorbance of the samples was measured with a spectrophotometer at a wavelength of 450–500 nm with the reference absorbance at 630–690 nm. The mean and standard deviation of triplicates were calculated and plotted.

2.6 *In vitro* PERS observation

PERS spectra were obtained from the Fu-AuNP treated cells which were cultured on a glass cover slip and transferred into a homemade live-cell chamber. PERS spectra were obtained by a 1200 lines per mm grating using a Renishaw InVia Raman spectrometer (laser spot size $\sim 1.5 \mu\text{m}$) combined with a Leica microscope. A 532 nm excitation laser was directed through a series of reflecting lenses and apertures, which focused onto a $50\times$ objective. PERS signals were collected by using a CCD detector from $400\text{--}1800 \text{ cm}^{-1}$ with 10 s of integration time. Dark-field images were obtained by using a halogen lamp with a dark-field condenser which was placed at the bottom of a living cell chamber. All collected PERS data was measured from ten independent cells with the Fu-AuNPs' concentrated positions from dark-field observation.

3 Results and discussion

3.1 Synthesis and characterization of Fu-AuNPs

Fu-AuNPs were manufactured using a previously reported polysaccharide-mediated gold nanoparticle synthetic approach with a slight modification.^{30–32} Briefly, the appropriate concentration of a fucoidan extract solution was mixed with AuCl_4^- and incubated for 10 min at room temperature to ensure polysaccharide–metal cation complex formation through electrostatic interactions. Subsequent incubation at 80°C for 2 h led to a reduction of bound Au^{3+} ions by the hydroxyl groups present in the fucoidan chain. During the reaction, the color of the solution gradually changed from transparent to red, confirming the formation of plasmonic Au nanoparticles. Based on UV-Vis spectrophotometry measurements, Fu-AuNPs exhibited absorption maxima at 531 nm, and the extinction spectrum coincided with the appearance of color. After purification to remove any unreacted fucoidan extract, we assessed the diameter and morphology of the Fu-AuNPs using transmission electron microscopy (TEM) and dynamic light scattering (DLS). By optimizing the reaction conditions to control the nanoparticle diameter, we successfully prepared Fu-AuNPs with a core diameter of $35 \pm 1.9 \text{ nm}$ ($n = 100$, counting from TEM images) (Fig. 1b). The relatively larger hydrodynamic radius of the Fu-AuNPs ($50 \pm 10.3 \text{ nm}$ with a polydispersity index of 0.113, triplicate samples) implied attachment of the fucoidan chains to the surface of the nanoparticles (Fig. 1c).

3.2 Cell viability assay

Prior to the treatment of cells with Fu-AuNPs to induce autophagy, we performed a cytotoxicity assay in human oral squamous carcinoma cells (HSC3) using an XTT assay in order to optimize the concentration of Fu-AuNPs required to induce autophagic apoptosis. HSC3 cell viability was observed to decrease in

proportion to the concentration of Fu-AuNPs. Based on this observation, we selected a concentration of 100 μM at which more than 40% of the HSC3 cells underwent apoptosis (Fig. S1, ESI[†]). This concentration also produced virtually no scattering noise, therefore making it optimal for following cell-based autophagy. The HSC3 cell-based experiments were carried out using a red fluorescent protein (RFP)-labeled LC3B as a means to track autophagosomes in order to obtain evidence that autophagy is induced by Fu-AuNPs. This approach for studying autophagy has been very well described in the literature.^{33,34} Based on the fluorescence microscopy images, only Fu-AuNP-treated HSC3 cells expressed red fluorescence in the perinuclear region indicative of RFP-LC3B staining and it clearly supported the notion that Fu-AuNPs could induce autophagy (Fig. S2, ESI[†]).

3.3 Autophagy tracking by PERS

In order to perform real-time PERS, as well as dark field observation, we cultured HSC3 cells on glass cover slips and treated them with 100 μM Fu-AuNPs. The cells were then analyzed using our in-house live cell Raman platform. In order to minimize the effect of factors other than the Fu-AuNPs on the induction of autophagy, Raman spectroscopy continuous measurements were performed at a constant temperature of 37°C and with an appropriate nutritional supply.

Generally, when an exogenous material is introduced to cells, the material must first diffuse through the medium and approach the surface of the cell (the cell membrane) for internalization. In this cell membrane approaching phase, plasmonic Fu-AuNPs would be expected to first adsorb to the outer leaflet of the phospholipid bilayer, resulting in changes in the Raman spectrum derived from the phospholipid (Fig. 2a). It would be expected that the magnitude of these changes would increase in proportion to the cell surface accumulation of Fu-AuNPs. Accordingly, peaks at 718 cm^{-1} (phospholipid C–N stretching),^{35,36} 853 cm^{-1} (carbohydrate C–O–C stretching),³⁷ 1031 cm^{-1} (phospholipid C–N stretching),^{38,39} and 1337 cm^{-1} (amide III)⁴⁰ gradually increased and sharpened over the first three hours

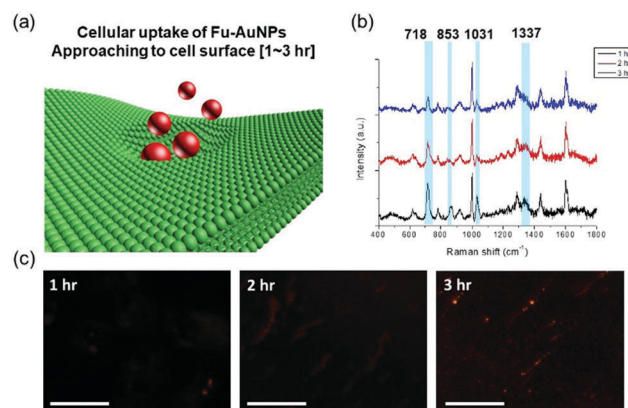


Fig. 2 Approaching the cell surface phase. (a) Schematic illustration of approaching the cell surface which occurs 1–3 h after Fu-AuNP treatment to HSC3 cells. (b) Measured Raman spectra and (c) dark field images presenting time-dependent accumulation of Fu-AuNPs on the cell surface. The scale bar is $50 \mu\text{m}$.

(Fig. 2b). Although the presence of Fu-AuNPs on the cell surface was not sufficient to obtain a clear plasmonically enhanced spectrum, it was possible to distinguish the phospholipid spectrum between the different noise spectra. Dark field images also showed that the concentration of Fu-AuNPs on the cell surface increased gradually (Fig. 2c).

We considered the period 3–6 hours after Fu-AuNPs treatment to be the endocytosis phase (Fig. 3a). In this phase, Fu-AuNPs adsorbed on the cell surface are engulfed into the cells and become trapped inside the endosome. During this process, Fu-AuNPs attached to the cell surface lipid bilayer were encapsulated with serum proteins from the cell culture medium, and detached from the internal endosome lipid surface. The previously observed Raman peak at 718 cm^{-1} representing phospholipid C–N stretching fluctuated presumably due to partial detachment from the interior surface of the endosome, and new peaks appeared at 500 cm^{-1} (protein disulfide bonds),^{41,42} 874 cm^{-1} (protein C–C stretching of hydroxyproline & ring deformation of tryptophan),⁴³ and 1210 cm^{-1} (C–H bending and C–C stretching of tyrosine, phenylalanine, and tryptophan) arising from the trapped biomolecules^{44,45} (Fig. 3b). From the dark field image, a bright dot pattern started to be visible in the cytoplasmic region, which gradually increased in strength, confirming the progress of endocytosis. The dark field imaging also revealed that these early endosomes were mainly located at the edge of the cytoplasm and gradually moved to the inside of the cell, over time (Fig. 3c). The cellular surface approach, endosome entrapping, and accumulation was additionally observed by means of bio-TEM images (Fig. S3, ESI†).

We considered the period 7–12 hours from treatment as the phase representing clustering of the Fu-AuNPs in the endosome (Fig. 4a). No specific peak enhancement or attenuation was observed during this process, whereas fluctuations in several minor peaks except 500 cm^{-1} , 1003 cm^{-1} , and 1585 cm^{-1} , which represent disulfide bonds and phenylalanine, occurred (Fig. 4b).

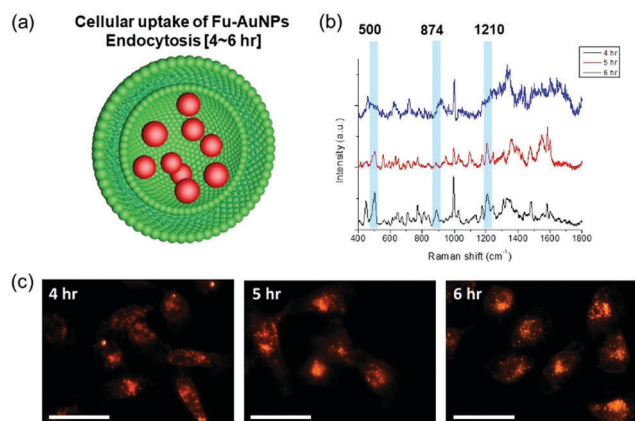


Fig. 3 Endocytosis phase. (a) Schematic illustration of endocytosis which occurs 4–6 h after Fu-AuNPs treatment to HSC3 cells. (b) Measured Raman spectra and (c) dark field images presenting encapsulation of Fu-AuNPs by endocytosis and the following signal increase of 500 , 874 and 1210 cm^{-1} from disulfide bonds and amino acids. Blue region implies the increase of the PERS signal. The scale bar is $50\text{ }\mu\text{m}$.

Typically, the drastic fluctuation of peaks at 724 cm^{-1} (DNA/RNA adenine ring breathing), 935 cm^{-1} (stretching mode of phospholipid), 1150 cm^{-1} (thymine, cytosine, C–O–C ring vibration), and $1360\text{--}1440\text{ cm}^{-1}$ (guanine, CH_2 bending of proteins/lipids) suggested that the migration of nanoparticle clusters and the influx of proteins and oligonucleotides into the endosome were occurring randomly in this period. It was not possible to directly observe the behavior of the nanoparticles in the endosome, but we could infer that the Fu-AuNPs aggregated inside the endosome to form a nano-sized gap in clusters for additional enhancement of Raman spectra. Comparing the Raman spectra six and seven hours after particle treatment, it could be seen that the standard deviation between the measured spectra was significantly reduced and the spectra were stabilized (Fig. 4c). Dark field images confirmed that the endosomes had migrated within the cytoplasm and collected in the peri-nuclear region where autophagy is known to occur (Fig. 4d).

Actual lysosomal fusion and the resulting autophagy were observed 13–24 hours after the treatment of HSC3 cells with Fu-AuNPs. A gradual disappearance of the Raman peaks at 500 cm^{-1} (disulfide bonds), 838 cm^{-1} (tyrosine), 1003 cm^{-1} (phenylalanine), 1210 cm^{-1} ($\text{C}_6\text{H}_5\text{--C}$ stretching of phenylalanine)

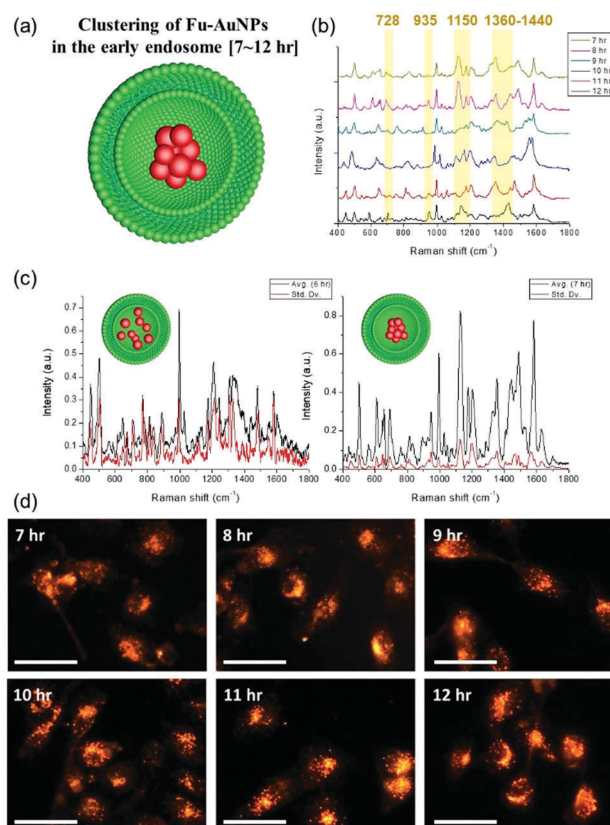


Fig. 4 Clustering of introduced Fu-AuNPs in the early endosome. (a) Schematic illustration of Fu-AuNP clustering which occurs 7–12 h from Fu-AuNP treatment to HSC3 cells. (b) Measured Raman spectra and (c) spectra with standard deviation plotting. Through the clustering process, the peaks were stabilized and (d) the dark field images exhibited migration of Fu-AuNPs containing vesicles to the peri-nuclear region for the following autophagosome–lysosome fusion step. The scale bar is $50\text{ }\mu\text{m}$.

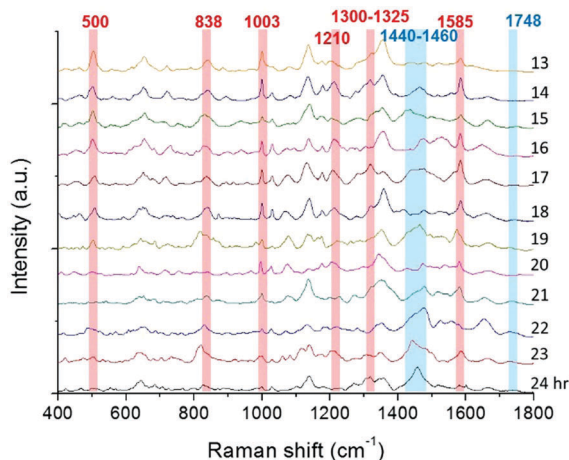


Fig. 5 Raman spectra during autophagy of HSC3 cells by Fu-AuNP treatment. Decrease of the peaks from DNA and peptides indicated protein denaturation and DNA fragmentation.

and tyrosine), $1300\text{--}1325\text{ cm}^{-1}$ ($-\text{CH}_2$ twisting of proteins) and 1585 cm^{-1} (phenylalanine & exposure of DNA bases) implied that protein denaturation and DNA fragmentation occurred during the autophagic apoptotic process.^{27,45,46} The signal increase at $1440\text{--}1460\text{ cm}^{-1}$ and 1748 cm^{-1} observed after 20 hours represented

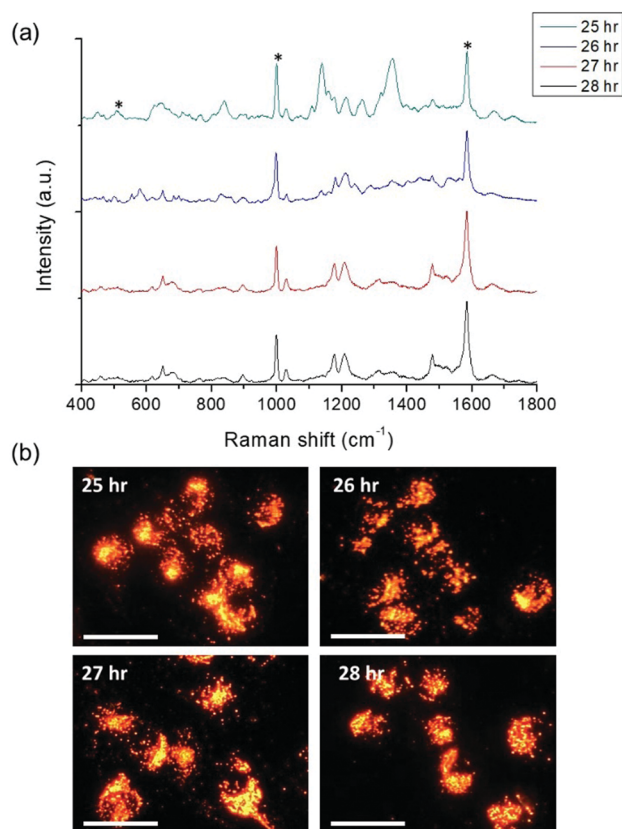


Fig. 6 Autophagic apoptosis of HSC3 cells. (a) Measured Raman spectra did not indicate further change after 26 h from the treatment of Fu-AuNPs, and it implied completion of the apoptosis process. (b) Dark field images exhibiting that recovery of the bright dot signals from the cytosolic region might originate from autophagosome degradation. The scale bar is $50\text{ }\mu\text{m}$.

the CH_2 -bending mode of proteins & lipids along with methylene deformation and lipid protein amide I, respectively^{46–48} (Fig. 5). These peaks are presumed to be due to cell shrinkage or autolysosome collapse at the apoptosis stage resulting from autophagy progression, followed by reunion to proteins and lipids. The dark field images also supported this conclusion (Fig. S4, ESI†). A bright dot pattern, which was initially dispersed in the perinuclear region, gradually coalesced into a small region, from which we deduced that the autolysosome was formed and that autophagy has occurred.

Moreover, after 20 hours, the dark field images revealed that the previously bright signals appeared to be coalesced together and had a much stronger intensity.

After 26 hours, no further Raman spectral changes were observed, indicating the completion of apoptosis (Fig. 6a). The significant increase in the peaks at 1003 cm^{-1} and 1585 cm^{-1} observed at 25 hours might have originated from autolysosome degradation and re-exposure of the Fu-AuNPs to the cytosol. Based on previous reports, the disappearance of the 500 cm^{-1} (disulfide bond) peak and the sharp 1003 cm^{-1} and 1585 cm^{-1} (phenylalanine) peaks are regarded as death markers in apoptotic cells.^{27,45,46} By this stage, the dark field signals were observed sporadically in the cytoplasmic region, suggesting that the Fu-AuNPs had escaped from the autolysosome and had become re-dispersed in the cell (Fig. 6b).

4 Conclusions

Using plasmonic nanoparticles coated with fucoidan, an autophagy inducing biopolymer, we were able to observe the autophagy of HSC3 cells and the resulting apoptosis process in real-time. The present platform is significant in that conventionally discrete induction and observation of biological phenomena can be easily combined using specific bio-nanomaterial complexes. Through a combination of PERS and dark field imaging, the whole autophagic process including internalization of the nano-complex, cytosolic migration, autophagy, and autophagic apoptosis could be continuously observed. As a result, the tracking of autophagy with a focus on changes at the molecular level was successfully accomplished, and we believe that the PERS technique using bioactive molecule–nanoparticle complexes could be useful in a variety of important research areas such as the real-time observation of stem cell differentiation regulation and the cell life cycle under specific conditions.

Conflicts of interest

There are no conflicts to declare.

Acknowledgements

This work was supported by the National Institute of Health (NIH)-National Cancer Institute (NCI) grant (U01CA151802). This study was supported by the National Research Foundation of Korea (NRF) funded by the Korean government (Grant No. NRF-2016R1C1B1008090).

Notes and references

- 1 B. Levine and D. J. Klionsky, *Dev. Cell*, 2004, **6**, 4763–4773.
- 2 X. Qu, Z. Zou, Q. Sun, K. Luby-Phelps, P. Cheng, R. N. Hogan, C. Gilpin and B. Levine, *Cell*, 2007, **128**(5), 931–946.
- 3 E. H. Baehrecke, *Nat. Rev. Mol. Cell Biol.*, 2005, **6**, 505–510.
- 4 J. Debnath, E. H. Baehrecke and G. Kroemer, *Autophagy*, 2005, **1**, 66–74.
- 5 S. Reef, E. Zalcvar, O. Shifman, S. Bialik, H. Sabanay, M. Oren and A. Kimchi, *Mol. Cell*, 2006, **22**(4), 463–475.
- 6 R. Mathew, S. Kongara, B. Beaudoin, C. M. Karp, K. Bray, K. Degenhardt, G. Chen, S. Jin and E. White, *Genes Dev.*, 2007, **21**(11), 1367–1381.
- 7 C. De Duve and R. Wattiaux, *Annu. Rev. Physiol.*, 1966, **28**, 435–492.
- 8 A. Kierszenbaum, *Histology and Cell Biology – An Introduction to Pathology*, Elsevier Saunders, Philadelphia, 2012.
- 9 L. M. Schwartz, S. W. Smith, M. E. Jones and B. A. Osbroune, *Proc. Natl. Acad. Sci. U. S. A.*, 1993, **90**(3), 980–984.
- 10 R. Mathew, V. Karantza-Wadsworth and E. White, *Nat. Rev. Cancer*, 2007, **7**, 961–967.
- 11 P. Boya, R. A. González-Polo, N. Casares, J. L. Perfettini, P. Dessen, N. Larochette, D. Métiver, D. Meley, S. Souguere, T. Yoshimori, G. Pierron, P. Codogno and G. Kroemer, *Mol. Cell Biol.*, 2005, **25**(3), 1025–1040.
- 12 W. X. Ding, H. M. Ni, W. Gao, T. Yoshimori, D. B. Stolz, D. Ron and X. M. Yin, *Am. J. Pathol.*, 2007, **171**(2), 513–524.
- 13 U. B. Pandey, Z. Nie, Y. Batlevi, B. A. McCray, G. P. Ritson, N. B. Nedelsky, S. L. Schwartz, N. A. DiProspero, M. A. Knight, O. Schuldiner, R. Padmanabhan, M. Hild, D. L. Berry, D. Garza, C. C. Hubbert, T. P. Yao, E. H. Baehrecke and J. P. Taylor, *Nature*, 2007, **447**, 859–863.
- 14 D. C. Rubinsztein, *Nature*, 2006, **443**, 780–786.
- 15 K. Degenhardt, R. Mathew, B. Beaudoin, K. Bray, D. Anderson, G. Chen, C. Mukherjee, Y. Shi, C. Gélinas, Y. Fan, D. A. Nelson, S. Jin and E. White, *Cancer Cell*, 2006, **10**(1), 51–64.
- 16 E. L. Eskelinen, *Autophagy*, 2008, **4**, 257–260.
- 17 I. Tanida, T. Yamaji, T. Ueno, S. Ishiura, E. Kominami and K. Hanada, *Autophagy*, 2008, **4**, 131–134.
- 18 N. Mizushima, A. Yamamoto, M. Matsui, T. Yoshimori and Y. Ohsumi, *Mol. Biol. Cell*, 2004, **15**, 1101–1111.
- 19 Y. Matsui, H. Takagi, X. Qu, M. Abdellatif, H. Sakoda, T. Asano, B. Levine and J. Sadoshima, *Circ. Res.*, 2007, **100**, 914–922.
- 20 K. Suzuki, T. Kirisako, Y. Kamada, N. Mizushima, T. Noda and Y. Ohsumi, *EMBO J.*, 2001, **20**, 5971–5981.
- 21 B. Kang, L. A. Austin and M. A. El-Sayed, *ACS Nano*, 2014, **8**(5), 4883–4892.
- 22 M. Aioub and M. A. El-Sayed, *J. Am. Chem. Soc.*, 2016, **138**, 1258–1264.
- 23 S. R. Panikkanvalappil, S. M. Hira and M. A. El-Sayed, *Chem. Sci.*, 2016, **7**, 1133–1141.
- 24 S.-Y. Ding, J. Yi, J.-F. Li, B. Ren, D.-Y. Wu, R. Panneerselvam and Z.-Q. Tian, *Nat. Rev. Mater.*, 2016, **1**, 1–16.
- 25 B. Kang, L. A. Austin and M. A. El-Sayed, *Nano Lett.*, 2012, **12**, 5369–5375.
- 26 S. R. Panikkanvalappil, S. M. Hira, M. A. Mahmoud and M. A. El-Sayed, *J. Am. Chem. Soc.*, 2014, **136**, 15961–15968.
- 27 S. R. Panikkanvalappil, M. A. Mahmoud, M. A. Mackey and M. A. El-Sayed, *ACS Nano*, 2013, **7**(9), 7524–7533.
- 28 K. W. Lee, D. Jeong and K. Na, *Carbohydr. Polym.*, 2013, **94**, 850–856.
- 29 K. Senthilkumar, P. Manivasagan, J. Venkatesan and S.-K. Kim, *Int. J. Biol. Macromol.*, 2013, **60**, 366–374.
- 30 H. Jang, Y.-K. Kim, S.-R. Ryoo, M.-H. Kim and D.-H. Min, *Chem. Commun.*, 2010, **46**, 583–585.
- 31 H. Jang, S.-R. Ryoo, K. Kostarelos, S. W. Han and D.-H. Min, *Biomaterials*, 2013, **34**(13), 3503–3510.
- 32 H. Jang, K. Kang and M. A. El-Sayed, *J. Mater. Chem. B*, 2017, **5**, 6147–6153.
- 33 S. Kimura, T. Noda and T. Yoshimori, *Autophagy*, 2007, **3**(5), 452–460.
- 34 N. Mizushima, T. Yoshimori and B. Levine, *Cell*, 2010, **140**(3), 313–326.
- 35 K. Czamara, K. Majzner, M. Z. Pacia, K. Kochan, A. Kaczor and M. Baranska, *J. Raman Spectrosc.*, 2015, **46**, 4–20.
- 36 T. Meyer, N. Bergner, C. Bielecki, C. Krafft, D. Akimov, B. F. M. Romeike, R. Reichart, R. Kalff, B. Dietzek and J. Popp, *J. Biomed. Opt.*, 2011, **16**(2), 021113.
- 37 G. Shetty, C. Kendall, N. Shepherd, N. Stone and H. Barr, *Br. J. Cancer*, 2006, **94**(10), 1460–1464.
- 38 N. C. Maiti, M. M. Apetri, M. G. Zagorski, P. R. Carey and V. E. Anderson, *J. Am. Chem. Soc.*, 2004, **126**(8), 2399–2408.
- 39 T. G. Spiro, *Biological applications of Raman spectroscopy*, Wiley, Hoboken, NJ, 1987.
- 40 C. S. Teixeira, R. A. Bitar, H. S. Martinho, A. B. Santos, M. A. Kulcsar, C. U. Friguglietti, R. B. da Costa, E. A. Arisawa and A. A. Martin, *Analyst*, 2009, **134**(11), 2361–2370.
- 41 I. U. Rehman, Z. Movasaghi and S. Rehman, *Vibrational spectroscopy for tissue analysis*, CRC Press, Boca Raton, FL, 2013.
- 42 H. E. Van Wart, A. Lewis, H. A. Scheraga and F. D. Saeva, *Proc. Natl. Acad. Sci. U. S. A.*, 1973, **70**(9), 2619–2623.
- 43 Y. Wu, Y. Dong, J. Jiang, H. Li, T. Zhu and S. Chen, *Sci. Rep.*, 2017, **7**, 38706.
- 44 S. P. A. Fodor, R. A. Copeland, C. A. Grygon and T. G. Spiro, *J. Am. Chem. Soc.*, 1989, **111**(15), 5509–5518.
- 45 S. A. Asher, L. Michael and C. R. Johnson, *J. Am. Chem. Soc.*, 1986, **108**, 3186–3197.
- 46 S. R. Panikkanvalappil, M. A. Mackey and M. A. El-Sayed, *J. Am. Chem. Soc.*, 2013, **135**, 4815–4821.
- 47 E. B. Hanlon, R. Manoharan, T.-W. Koo, K. E. Shafer, J. T. Motz, M. Fitzmaurice, J. R. Kramer, I. Itzkan, R. R. Dasari and M. S. Feld, *Phys. Med. Biol.*, 2000, **45**(2), R1–R59.
- 48 C. Mattaus, B. Bird, M. Miljkovic, T. Chernenko, M. Romeo and M. Diem, *Methods Cell Biol.*, 2008, **89**, 275–308.